RESEARCH ARTICLE

Self-healing triggering mechanism in epoxy-based material containing microencapsulated amino-polysiloxane

Sara Ferreira Da Costa[1,2] | Marcus Zuber[3,4] | Margarita Zakharova[2] |
Andrey Mikhaylov[2] | Tilo Baumbach[3,4] | Danays Kunka[2] | Sergio Henrique Pezzin[1]

[1] Center of Technological Sciences, State University of Santa Catarina, R. Paulo Malschitzki, 200 - Zona Industrial Norte, Joinville, SC 89219-710, Brazil

[2] Institute of Microstructure TechnologyKarlsruhe Institute of Technology, Hermann-von-Helmholtz-Platz 1, Eggenstein-Leopoldshafen 76344, Germany

[3] Institute for Photon Science and Synchrotron RadiationKarlsruhe Institute of Technology, Eggenstein-Leopoldshafen D-76344, Germany

[4] Laboratory for Applications of Synchrotron Radiation (LAS), Karlsruhe Institute of Technology, Kaiserstr. 12, Karlsruhe D-76131, Germany

Correspondence
Sergio Henrique Pezzin, Universidade do Estado de Santa Catarina Joinville, SC 89219-710, Brazil.
Email: sergio.pezzin@udesc.br

Abstract

This work combines non-destructive X-ray micro-computed tomography (μCT) and scanning electron microscopy (SEM) to study the self-healing triggering mechanism in a system consisting of an epoxy resin, based on diglycidyl ether of bisphenol A, with embedded poly(urea-formaldehyde) (PUF) microcapsules filled with an amino-functional polysiloxane (PDMS-a) as a healing agent. μCT and SEM analyses proved that PDMS-a was effective in filling the microcrack areas, providing an efficient self-healing process, and confirmed that the main mechanisms for increasing fracture toughness are due to crack bowing and deflections. It was also observed that the diameter and shell thickness of the microcapsules are essential factors for their dispersion and integrity into the polymer matrix. PUF microcapsules with shell thickness of ca. 0.4 μm and diameters <60 μm were stable and well dispersed within the matrix. These findings shed light for understanding the increase of the fracture toughness, after self-healing, reported in our previous study of this system.

KEYWORDS

dgbea, epoxy, microcapsule, self-healing, triggering mechanism, X-ray micro-computed tomography

1 | INTRODUCTION

Self-healing materials autonomously or non-autonomously can repair surface and/or internal damages, avoiding failure by crack propagation and fracture, and recovering, partially or completely, mechanical, thermal, or electrical properties at the repaired area.[1–3] It is inevitable that, after some time, due to mechanical, thermal, and chemical factors or a combination of these, microcracks appear on the surface or the bulk of polymer materials.[4–6] To prevent their failure when in service and to reduce maintenance costs, various self-healing polymer materials, using autonomic or non-autonomic approaches, have been proposed and developed.[7]

There are two types of autonomous self-healing mechanisms: intrinsic and extrinsic. It is intrinsic when the healing process occurs by reversible covalent bonds or dynamic interactions caused by intermolecular forces.[8] In the extrinsic mechanism, self-healing occurs using microcapsules or vascular networks, where the microcrack growth triggers the self-healing process at room temperature. If the material needs an external stimulus such as heat,[9,10] light

or change of pH [11] to start the healing process, it is then a non-autonomous self-healing material.

The use of poly (urea-formaldehyde) (PUF) microcapsules filled with a liquid healing agent embedded in a polymer matrix is one of the most used extrinsic autonomous approaches. Generally, when a microcrack grows, it can eventually find a microcapsule, which breaks and releases a liquid self-healing agent, which reacts with the remaining functional groups of the polymer resin or a catalyst dispersed within the matrix, initiating a crosslinking process.[12] For this, the microcapsule's shell must remain intact during the manufacture of the sample, but easily ruptured by a crack. It is also necessary to have enough and well-dispersed microcapsules, since the volume of the encapsulated healing agent should be sufficient to crosslink the highest possible number of microcracks. Otherwise, if the crack passes through a region with no microcapsules, it continues propagating, and an abrupt rupture may occur throughout the material.[13,14]

The efficiency of the healing process evaluated by fracture toughness tests is commonly. The investigations are done using a tapered double cantilever beam (TDCB) or double cantilever beam geometry because the crack growth can be controlled along the sample center line.[2,15] These tests clearly shows that the healing efficiency is dependent on the content and size of microcapsules. With an increase in the diameter of the microcapsules, higher healing efficiencies are achieved,[2,15] at the cost of a decrease in the mechanical properties of the polymer.[13]

Epoxy resins are widely studied as matrices[16–18] in self-healing polymer materials, as, generally, there is no need for external intervention, other than microcracks, since the crosslinking can occur at room temperature. Usually, the use of catalysts is also not necessary, since the healing agents can react with residual amines or epoxy groups within the polymer matrix.[17,18] Amino-functional polysiloxane (PDMS-a) is a suitable healing agent, due to its reactive amine groups and greater thermal stability than the epoxy matrix; moreover, it gives a higher ductility to the healed region.[17,18]

In our previous work,[17] the fracture toughness of TDCB specimens of an epoxy resin-based on diglycidyl ether of bisphenol A (DGEBA) with PUF microcapsules (2.5 and 5 wt%), filled with PDMS-a and/or the resin hardener, was investigated. The results showed that the fracture toughness of the healed polymer is dependent on the total concentration of microcapsules and the type of healing agent. High healing efficiencies were obtained with 2.5 wt% of PDMS-a/TETA-filled microcapsules, but fracture toughness decreased with the use of 5 wt% microcapsules, in all cases, what can be directly related to the agglomeration of microcapsules.[17] Similar results have been reported on the effect of the microcapsule size in self-healing polymers. It was shown that samples with

10 wt% of microcapsules, with diameters of ca. 200 μm, presented low values of fracture toughness. The experiments also reveal that the maximum healing efficiency does not vary significantly with the change of the microcapsule size.[14] Several studies using the microcapsule approach have also shown that the self-healing efficiency is improved in systems with more than 3 wt% of microcapsules; however, at the expense of mechanical strength and thermal properties.[18–20] A recent work presented an innovative system using magnetic nanoparticles inside microcapsules. Epoxy systems containing 4 wt% of microcapules (with ca. 90 μm) proved to efficiently self-heal damages.[21]

Scanning electron microscopy (SEM) is the most widely used method to observe the fracture surface of the materials.[22] SEM helps to understand how the size of the microcapsules affects the mechanical properties of the polymer and how self-healing takes place, as well as to evaluate the adhesion of microcapsules in the matrix and the characteristics of the healed region.[23] However, the sample needs to be fractured, and normally only a small part of the polymer matrix is analyzed. An evaluation of these factors throughout the sample would allow improving the fabrication techniques of self-healing polymer materials, aiming at better mechanical performance and higher healing efficiency.[24]

On the other hand, X-ray micro-computed tomography (μCT) is a non-destructive technique that can be also effectively employed to evaluate self-healing materials, allowing bulk visualization by 3D reconstruction.[25,26] μCT is a versatile, non-destructive, experimental technique that can display morphological features within non-optically transparent materials, like polymers, and reconstruct their spatial characteristics. For instance, μCT was applied to evaluate the rupture of solvent-filled microcapsules in the fracture region and quantify the healing agent released,[27,28] detecting healed and non-healed areas. Mayo et al. characterized PUF microcapsules with encapsulated dichlorobenzene (DCB), dispersed in a poly(methylmethacrylate)-polystyrene matrix. The sample was fractured and self-healed at room temperature for 7 days. Through the slices obtained in the analysis, the authors were able to distinguish microcapsules filled with DCB from the polymer matrix and broken microcapsules.[27,28] Mookhoek et al.[28] analyzed a self-healing sample by tomography using synchrotron radiation and found that the rate of increased absorption after fracture depends on the diameter of the microcapsule, showing a delay for larger microcapsules due to their small surface/volume ratio.[28] In a recent work, Caballero-Peñas et al. studied the self-healing of epoxy samples, with different curing agents, after performing a superficial cut and heating the sample above its T_g. The results showed that free OH groups are responsible for self-healing, and the authors pointed to the need to evaluate
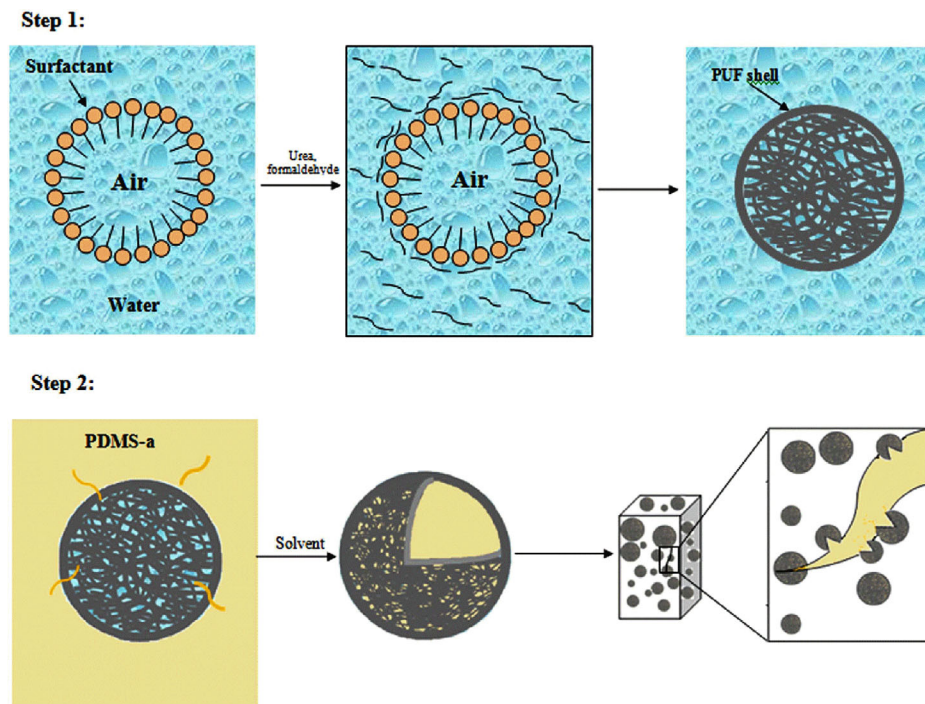
FIGURE 1 Scheme showing the synthesis of PUF microcapsules. Step 1 (upper figure): the surfactant dissolved in water forms a water-air colloidal suspension and the shell is then formed on the surface of entrained air bubbles; step 2 (lower figure): since the shell is porous, the hollow microcapsules are mixed with PDMS-a and the healing agent infiltrated by vacuum

larger areas to confirm self-healing mechanisms.[29] It is also possible to follow the crack propagation as a mechanical test is performed, enabling obtaining information in situ about how microcapsules are broken, how the healing agent fills the cracks, and self- healing efficiency.[30] However, there are still no works reporting the use of μCT to the study of self-healing systems using microencapsulated polysiloxane as healing agents.

This work presents a study of the self-healing mechanism in an epoxy matrix, using microencapsulated PDMS-a as a healing agent, by analyzing specimens after mechanical stress. By combining μCT with morphological analysis, it was possible to assess the distribution and stability of the microcapsules, as well as to identify the trigger mechanism when a crack appears within the matrix, evidencing that PDMS-a was capable of self-healing microcracks even at room temperature. These results shed light on the understanding of our previous findings on these systems.[17]

2 | EXPERIMENTAL SECTION

2.1 | Materials

Epoxy resin Renlam M, based on diglycidyl ether of bisphenol A ($C_{21}H_{24}O_4$, DGEBA), and its hardener Aradur 956-2 ($C_6H_{18}N_4$), composed of aliphatic polyamine (TETA),

were provided by HUNTSMAN (Brazil). For the synthesis of hollow microcapsules, sodium lauryl sulfate ($C_{12}H_{25}NaO_4S$, 99% purity) (SLS), formaldehyde (CH_2O, 37% in H_2O), ammonium chloride (NH_4Cl, >99%), urea (CH_4N_2O, >99%), sodium hydroxide (NaOH, PA), resorcinol ($C_6H_6O_2$, PA), hydrochloric acid (HCl, 37%) and octanol ($C_8H_{18}O$, >99%) were all purchase from Vetec (Brazil) and used as received. An aminated polydimethylsiloxane (PDMS-a) (BELSIL ADM 1370, Wacker, Germany) was used as a healing agent, having a viscosity of ca.1550 mPa.s and an amine number of 0.6 meq g^{-1} (information provided by the supplier). Chloroform (VETEC) was used to isolate the microcapsules by vacuum filtration.

2.2 | Synthesis of poly(urea-formaldehyde) (PUF) microcapsules

Hollow PUF microcapsules were synthesized through a water-air colloidal suspension (Figure 1, step 1) based on the method described by Brown et al.[31] and Blaiszik et al.,[32] with modification of the surfactant and the agitation speed.[17]

In a 500 mL jacketed reactor, 0.4 g SLS (surfactant) was dissolved in 200 mL deionized water by a digital mechanical stirrer (FISA model 713D) with an agitation

rate of 800 rpm. In this step, the air micro-bubbles are formed.[11] Crosslinking agents–urea (5 g), ammonium chloride (0.5 g), and resorcinol (0.5 g)—were added and the pH, verified by a pH meter (OAKTON, 510 series), adjusted to 3.5 using HCl (0.1 mol L^{-1}). After 10 minutes, formaldehyde was added to the suspension, and the temperature adjusted to 55°C to start the reaction. The PUF shells (hollow microcapsules) are then formed on the surface of entrained air bubbles. After 4 hours of reaction time, the microcapsules were rinsed with deionized water and filtrated under vacuum (filter paper with a pore size of 8 μm). The capsules were then air-dried for 24 hours, which resulted in a free-flowing powder.

The hollow microcapsules were then mixed with the healing agent (PDMS-a) in a Kitasato flask, and the mixture stirred under vacuum for 5 hours, following the procedure described by Jin et al.[33] The microcapsules were then rinsed with chloroform to remove excess, non-encapsulated PDMS-a, and immediately used for the preparation of the specimens. Studies on the necessary time for the effective infiltration of the microcapsules, as well as the more appropriate solvent to rinse them, are in the Supporting Information addressed, Sections S1 and S2, Figure S1 and S2. Analyses by optical microscopy showed that the optimal time for the infiltration of the microcapsules was approximately 5 hours.

2.3 | Morphology and thermal stability of microcapsules

An optical Olympus microscope (model CX31) and Field Emission Gun Scanning Electron Microscopy (FESEM, JEOL JSM 6701F) observed the morphology of hollow and filled microcapsules. For the optical images, the hollow microcapsules (~0.3 g) were dispersed in water (~40 mL) and a small aliquot placed on an uncoated glass plate. Subsequently, the average diameter and standard deviation of a minimum of 100 microcapsules were determined using the ImageJ (NIH, USA) software. Optical microscopy was also used to track the infiltration of PDMS-a, by the acquisition of multiple images over time. For FESEM, the microcapsules were dispersed in water and an aliquot was dropped on a carbon adhesive tape and dried for 24 hours. After this step, the samples were sputter-coated with a thin layer of gold. Energy Dispersive X-Ray Spectroscopy (EDX) qualitatively determined the core content of the microcapsules.

The thermal stability of hollow and filled microcapsules was measured by thermogravimetry (TG) using a NETZSCH equipment (STA 449C-JUPTER) with a heating rate of 10°C min^{-1}, in an atmosphere of N_2(g), from room temperature (25°C) to 600°C.

2.4 | Fabrication of the epoxy specimen containing filled microcapsules

The specimen was prepared by dispersing microcapsules (28 wt%) filled with PDMS-a within epoxy resin using a magnetic stirrer (IKA C-MAG HS7). The entrapped air was removed by slow stirring under vacuum for 1 hour. After dispersion, the hardener was added in a 5:1 weight ratio (as recommended by the supplier). The mixture was then poured by casting in a silicon mold, cured at room temperature and removed from the mold after 24 hours followed by 1 hours of post-cure at 100°C.

2.5 | Preparation of the specimen for X-ray micro-computed tomography (μCT) analysis

The self-healing specimen, with dimensions of ca. 9.5 mm (width) x 3 mm (thickness) x 36.0 mm (length) (Figure 2A), was fractured in a manual compression-testing machine (Paul Otto Weber) at 10 kN (Figure 2B). The specimen was fractured in two parts and one of them taken for analysis. The sample analyzed had approximately 9.5 mm length (Figure 2C).

2.6 | Characterization of fractured specimens by scanning electron microscopy (SEM)

Acquisition of images to investigate the fracture surface of epoxy specimens embedded with hollow or filled microcapsules was performed using a Zeiss Supra 60VP microscope at 5 keV.

2.7 | Nondestructive analysis by X-ray micro computed tomography

X-ray Micro-computed Tomography (μCT) analyses of the fractured self-healing specimen were performed at the Computed Lamiography/Computed Tomography Lab of the Institute for Photon Science and Synchrotron Radiation (IPS) at the Karlsruhe Institute of Technology (KIT). The laboratory source was a microfocus X-ray tube (X-RAY WorX) with a tungsten target. The X-ray tube was operated at 50 kV with a target power of 10 W, to achieve a focal spot size of 7 μm. The samples with microcapsules were imaged with a Dexela 1512 CMOS X-ray detector coupled to a CsI scintillator, with a physical pixel size of 74.8 μm. A cone-beam geometry was used to enable a magnification (M) of
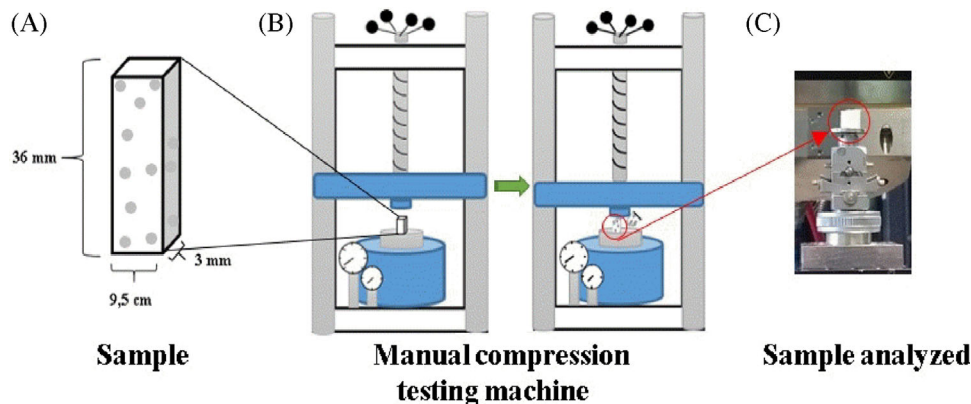
FIGURE 2 A, Scheme presenting the self-healing sample with 28 wt% embedded microcapsules and its dimensions; B, sample fracture in a compression testing machine, and C, fragment chosen for further µCT analysis
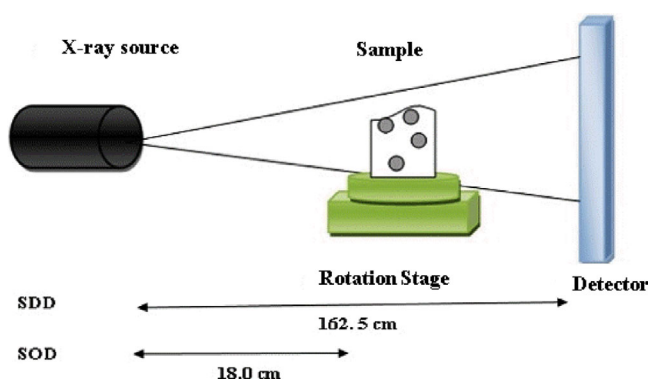

FIGURE 3 µCT setup, consisting of an X-ray tube, rotation stage, and detector, in which SDD is the distance from the source to the detector, and SOD is the distance from the source to the object (sample). The sample is placed on the rotation stage between the source and the detector
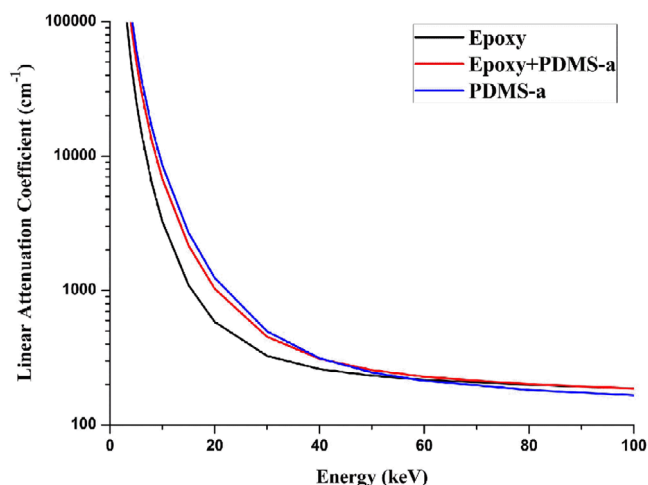

FIGURE 4 Variation of total attenuation coefficient with photon energy for DGEBA, PDMS-a and a mixture of both. The data were extracted from XCOM web-database of the National Institute of Standards and Technology (NIST)

the sample image, which can be calculated as follows:

$$M = SDD/SOD \tag{1}$$

where SDD is the distance from the source to the detector, and SOD is the distance from the source to the object. The SDD was set to 162.5 cm for tomographic measurements. The SOD was adjusted to improve the initial resolution of the imaging setup by adapting the magnification, while keeping the field of view large enough to image the whole sample. For the imaging, SOD was set to 18 cm for the samples with microcapsules. These manipulations resulted in the effective pixel of 8.3 µm for the tomographic measurements. The experimental setup is illustrated in Figure 3. For each measurement, a series of 2048 frames (projections) were taken over a 360° angular range with an exposure time of 2 seconds per frame. Octopus software was used for data reconstruction. Visualization and analysis of the images of slices and the 3D reconstruction was performed employing ImageJ (NIH, USA).

2.8 | Image analysis procedure of the microcapsule/polymer system

The images acquired by X-ray µCT were first analyzed to distinguish volume discontinuities (pores, ruptured microcapsules) from filled microcapsules and the epoxy matrix, by considering the differences between the attenuation coefficients of the materials that make up the self-healing system (basically epoxy and PDMS-a). The total attenuation coefficients of these materials at different energies (from 1 to 100 keV), obtained from the XCOM web-database of the National Institute of Standards and Technology (NIST),[25,34] is plotted in Figure 4.
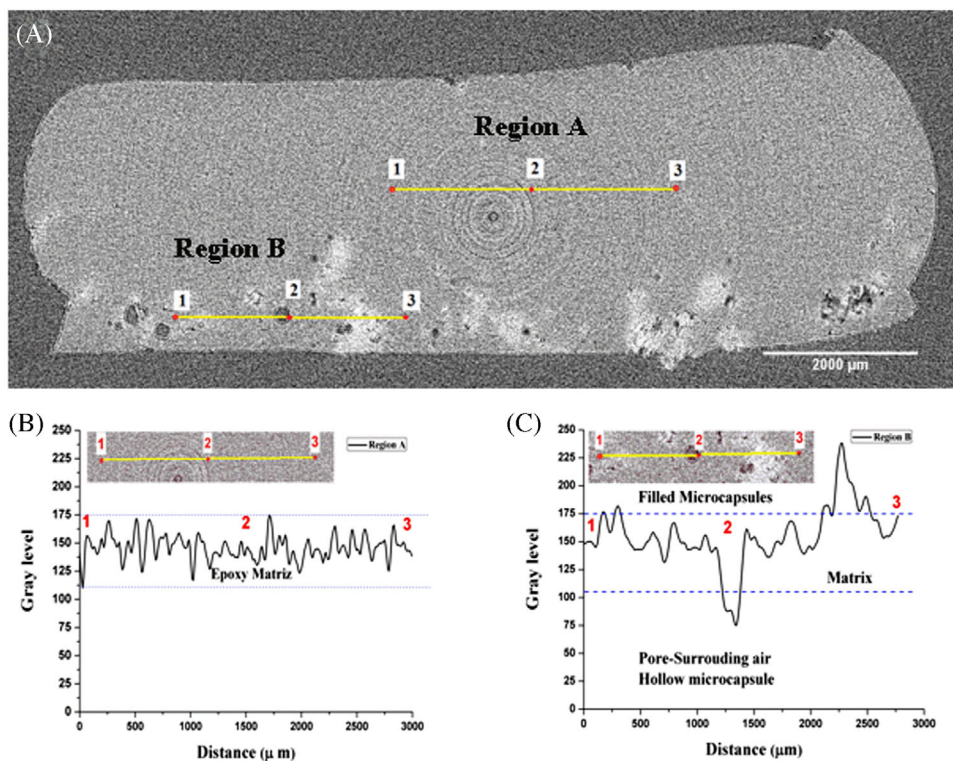
FIGURE 5 A, Grayscale image of a slice of the epoxy specimen with embedded microcapsules (self-healing sample) showing the region chosen for the threshold; B, identification of region A through the grayscale threshold band set at 110-175 for the matrix, and (C) identification of region B through the grayscale threshold band set at 0-110 for air, 110-175 for matrix, and above 175 for PDMS-a/filled microcapsules

When comparing the epoxy matrix with the PDMS-a, Figure 4 shows that there is a reasonable difference in total attenuation between them for energies below 50 keV.

Considering these data and considering that the attenuation coefficient for air [34] is far below the values for DGEBA and PDMS-a, a grayscale analysis was carried out in the regions of a specimen highlighted in Figure 5A. The air (pores, ruptured microcapsules, etc.) appear dark, the polymer matrix is gray, and the microcapsules filled with PDMS-a appear in a light gray color.

These gray levels were then divided according to the profile analysis of the highlighted line in regions A and B, (Figure 5B,C, respectively), where OX-axis represents distance along the highlighted line and OY-axis represents pixel intensity in gray scale values, taking into consideration a 8-bit image, 0 to 255-grayscale range. The area of interest in region A is attributed to the polymer matrix, while the area of interest in region B intercepts the polymer matrix, a ruptured microcapsule and filled microcapsules. Thus, grayscale values in range from 0 to 110 could be associated with surrounding air, pores, or hollow microcapsules, while values from 110 to 175 represent the epoxy matrix. The gray values above 175 are attributed to filled microcapsules and PDMS-a released within the epoxy matrix.

To better visualize and distinguish the different structures in the matrix, a binarization treatment was carried out using a discrimination analysis method.[35] The image processing for particle analysis is available in the, Section S3, Figure S3, and Supporting Information. By plotting the relative frequency histogram (Figure 6) and setting the threshold at values defined above (Figure 5), the structures of interest were segmented out of the image data. Density slicing using the grayscale thresholds yielded binary images differentiating polymer matrix (Figure S3a) and filled microcapsules (Figure S3b-c).

3 | RESULTS AND DISCUSSION

3.1 | Evaluation of the morphology and average size of hollow microcapsules

Figure 7 displays an optical micrograph of PUF microcapsules, showing size distribution and morphology. The hollow microcapsules (Figure 7A) have a spherical shape with sizes ranging from 13 to 127 μm, and an average diameter of 57 ± 26 μm (Figure 7B), compatible with other studies.[36] The thickness of the microcapsule shell is ca. 400 nm, as can be seen in Figure 7D. The formation of smaller capsules occurs near the propeller blades, where micro-scale eddies take place, while larger microcapsules are produced in the eddies away from the propeller.[37] During synthesis,
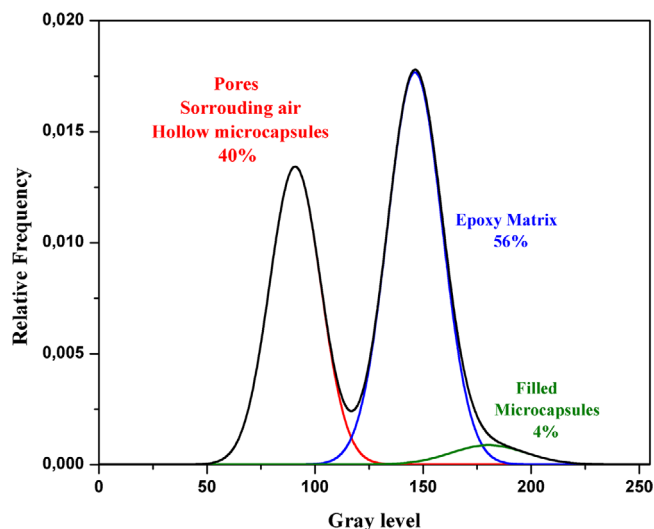
FIGURE 6 Relative frequency histogram of the slice of the epoxy matrix with microcapsules (Figure 5) with indicated gray value ranges representing voids (hollow microstructures, pores, air, and ruptured microcapsules), the epoxy matrix and filled microcapsules

some capsules reach the nanometer size and deposit on the microcapsule shell, increasing its thickness and roughness as observed by the SEM micrograph in Figure 7C. Other authors [38,39] also reported this behavior.

3.2 | Evaluation of the infiltration process

When the microcapsules are infiltrated, their color aspect change to transparent, while hollow or ruptured microcapsules appear dark, as can be noticed in Figure 8, although the black appearance can also be attributed to thicker walls.[40] The aspect of the microcapsule's shell (rough, smooth, intact, broken) can be also visualized by FESEM images, and semi-quantitative EDX analysis was used to indicate the presence of the healing agent (Figure 9). In the EDX spectrum, Figure 9A, the elements related to PUF: carbon (C), oxygen (O) and nitrogen (N) are present, as expected. The small signal just above 2 keV is related to Au (2.120 keV), from sample treatment by sputtering. The wt% values for each element are found in Table 1.

Figure 9B-C show the spectra of two microcapsules filled with the healing agent, but one of them is ruptured. The silicon (Si) found in the EDX analysis indicates the presence of PDMS-a and the amounts of Si in both samples are close to each other. In the analysis of the filled microcapsule (Figure 9B), no nitrogen was found, which means that the healing agent may have not been fully removed from the outside of the capsule during filtration, or was released

by the capsule's pores under vacuum (at the FESEM chamber). On the other hand, the EDX analysis performed within a ruptured microcapsule in Figure 9C exhibits N, related to PUF shell, and Si, from the healing agent. As the Si amount is much higher inside the microcapsule, there is an indication that it has been filled with PDMS-a.

TG analyses of PDMS-a, hollow microcapsules and microcapsules filled with PDMS-a are shown in Figure 10. The thermogram for hollow microcapsules has two main weight loss steps: the first with T$peak$ at 96°C with a 6 wt% loss, relative to elimination of free formaldehyde and adsorbed water; and the second at T$peak$ ~270°C, attributed to the fragmentation of the crosslinked structure of PUF, with a 73 wt% loss. At 600°C, there was still 22% of the initial weight. The healing agent decomposition starts at ~479°C and ends at ~508°C. The microcapsules filled with the healing agent show increased thermal stability when compared with the hollow microcapsule, as also observed for similar systems in the literature,[38,40,41,42] confirming the efficiency of the infiltration procedure.

3.3 | μCT analysis of the dispersion of microcapsules within the epoxy matrix

μCT is decisive to answer questions regarding the filling of the microcapsules embedded within the polymer matrix, its dispersion, and crack triggering, as this information are not entirely provided by optical microscopy or FESEM.[43,44] As already pointed out, the mechanical properties of the self-healing system strongly depend on the dispersion state and the strength of microcapsules in the polymer matrix.[14,17] The dispersion state of microcapsules is also crucial for the trigger mechanism, since, if a crack initiates and propagates through a volume without microcapsules filled with the healing agent, it will inexorably advance until the specimen is completely ruptured.

μCT analysis captures a series of projections during the rotation of the sample at 360 °, as shown in Figure 11. Figure 11 presents the top of the sample, which means the part of the sample that was in contact with air during the cure, the sample side (thickness of 3 mm), and its bottom, which means the area in contact with the mold during the cure. The self-healing sample is placed in the rotation stage (Figure 12A), where a series of 2D X-ray images (projections) are obtained. The software reconstructs the data in 2D cross-sections (or slices) of the sample. The total number of slices for this sample was 1277 (Figure 12B), from which 504 were chosen for the dispersion analysis of microcapsules. Subsequently, these slice images are reconstructed in 2D cross sections (Figure 12C) in the z direction. Markings on the sample help to visualize the front and side of the sample.
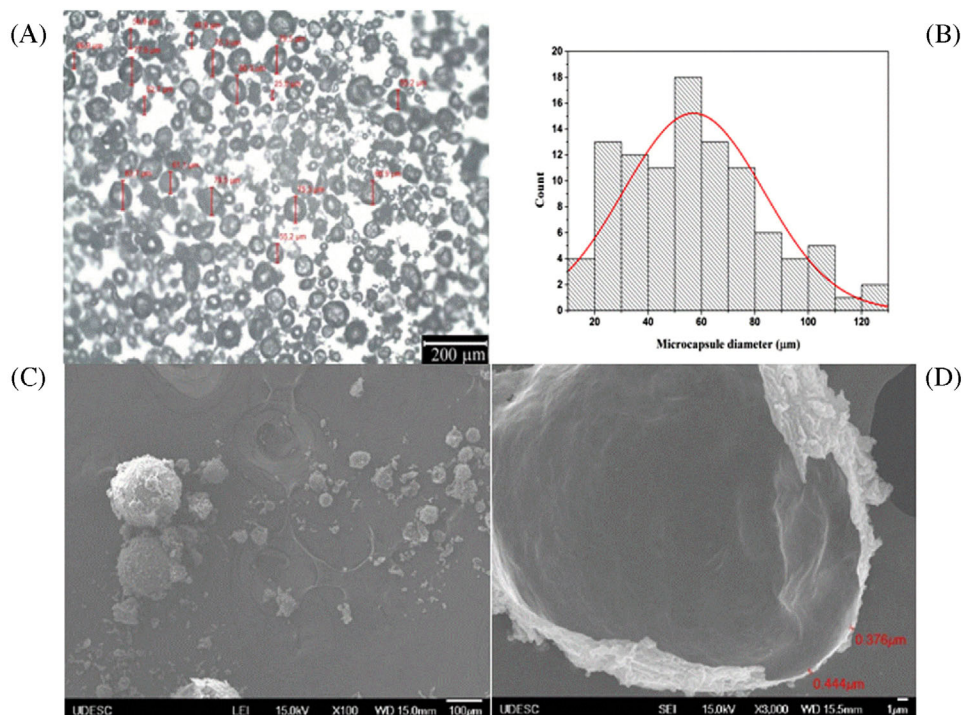
FIGURE 7 Morphology and the average size of hollow microcapsules: A, optical micrograph; B, size distribution of microcapsules prepared at 800 rpm; C, FESEM image showing different capsule sizes, and (D) FESEM image of a ruptured PUF microcapsule—shell thickness of ~400 nm
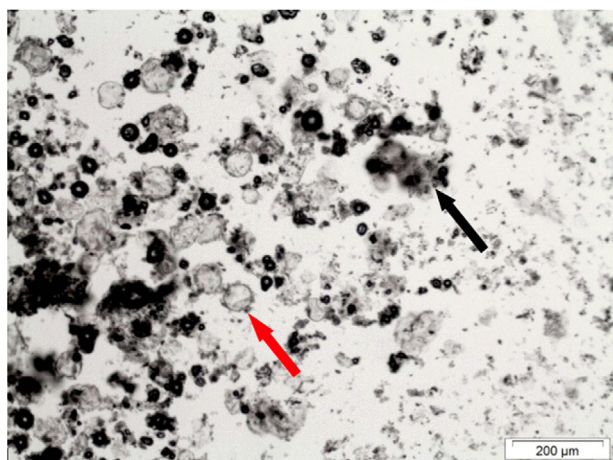
FIGURE 8 Optical micrograph of microcapsules filled with PDMS-a, highlighted by the red arrow. The black arrow highlights a ruptured microcapsule

TABLE 1 Elemental mass percentage obtained by EDX analysis (regions depicted in Figure 8)

	C	**N**	**O**	**Si**
Hollow microcapsule	35.74	23.74	40.15	0.37
Filled Microcapsule	61.19	–	20.67	18.14
Filled microcapsule after rupture	30.03	13.57	30.04	26.36

Figure 13 presents a slice of the sample with embedded microcapsules. The distribution of microcapsules into the polymer matrix is concentrated from the surface until approximately half of the sample bulk, where disperse microcapsules and clusters, which are highlighted by the arrows, can be observed. Darker-gray level dots (Figure 13A), noted near the surface and the center of the sample, indicate the presence of hollow microcapsules, even

allowing the visualization of their PUF shells. Converting the image into binary (Figure 13B), the epoxy matrix and filled microcapsules appear white, while pores and hollow microcapsules appear as black dots. Using the threshold values defined in Figure 5, it is possible to show only the filled microcapsules (white dots), as in Figure 13C. A region of interest (ROI) was selected for the analysis to reduce noise (Figure 13D). Particle size ranges and circularity values were chosen to separate the microcapsules by size and shape, which helps differentiate between microcapsules and clusters. The closer to 1.0, the more circular the particle (microcapsule) is. Thus, microcapsules were selected choosing a circularity between 0.8 and 1.0, while circularity values from 0.3 until 0.7 were assigned to irregularly shaped clusters. The full description of this analysis is found in Section S3.

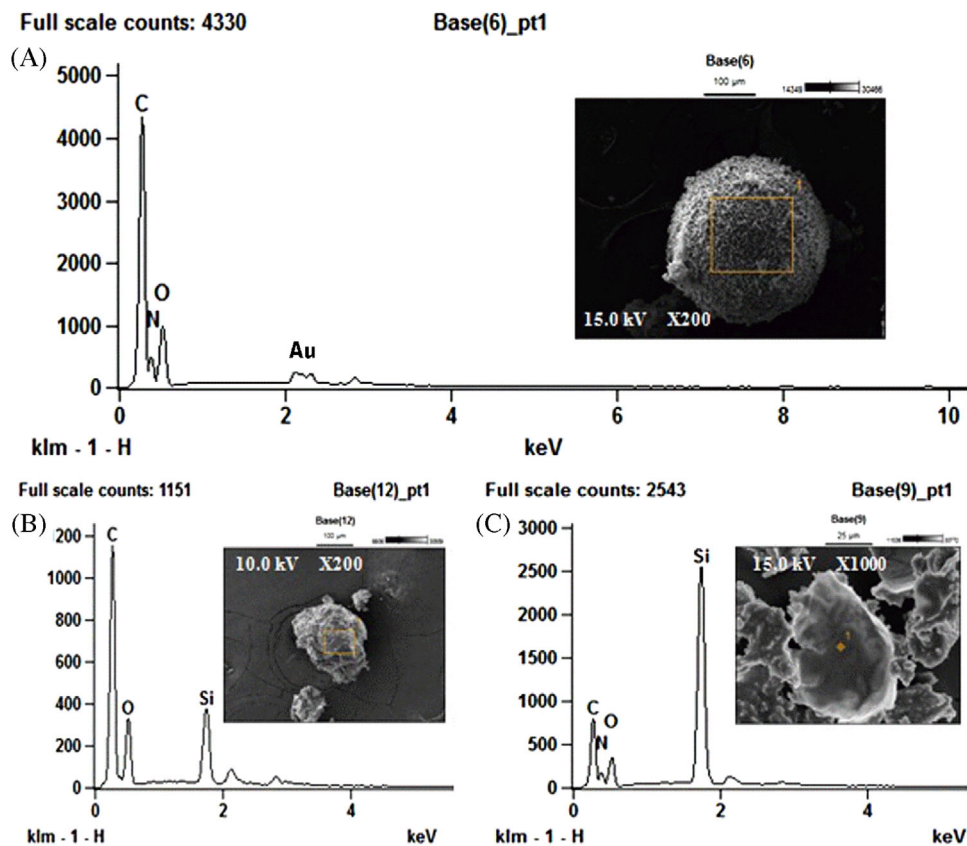The particle size distribution of the microcapsules embedded into the epoxy matrix, obtained from

FIGURE 9 EDX spectra and FESEM images of: (A) a hollow microcapsule; B, a microcapsule filled with the healing agent and (C) a filled microcapsule after rupture
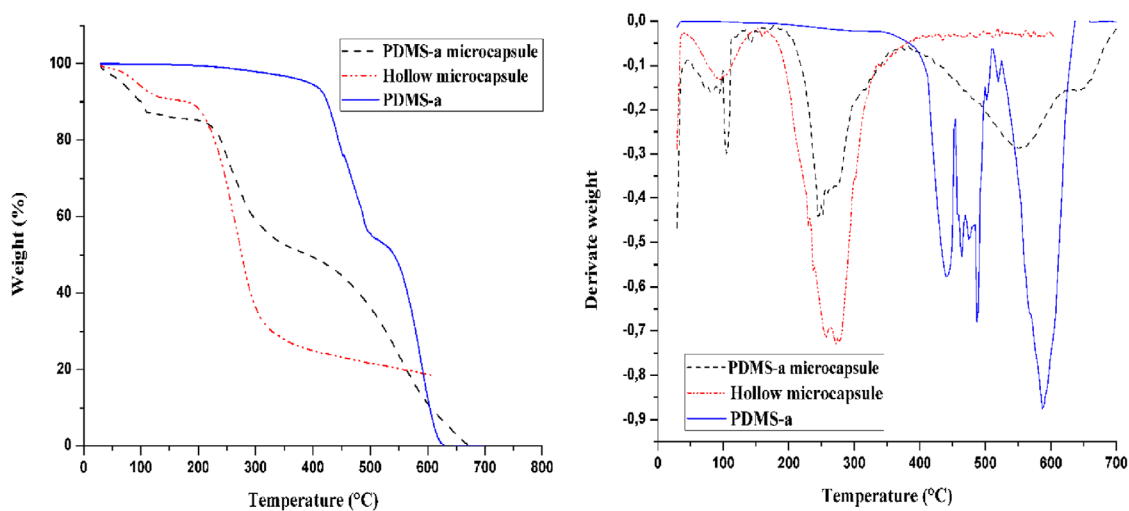

FIGURE 10 A, TG and (B) DTG curves for PDMS-a, hollow microcapsules, and PDMS-a filled microcapsules

Figure 13B-D, is presented in Figure 14. Through an analysis of the particle size distribution, the amount of filled and ruptured microcapsules can be estimated, as well as the presence of clusters within the polymer matrix.

It is observed an average particle size of 37 ± 24 μm for ruptured or hollow microcapsules embedded into the epoxy matrix, while the average size of microcapsules before mixing into the polymer was 57 ± 26 μm (Figure 7A). It is noteworthy that, after mixing, there are
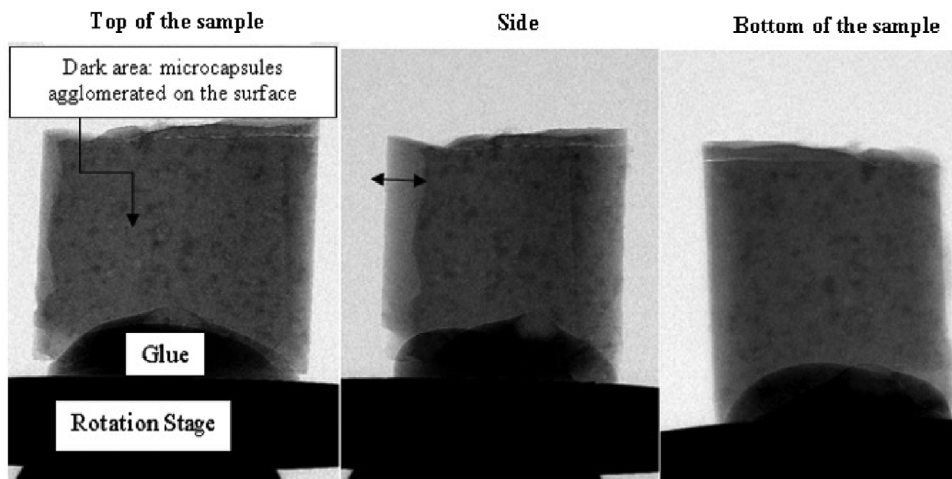
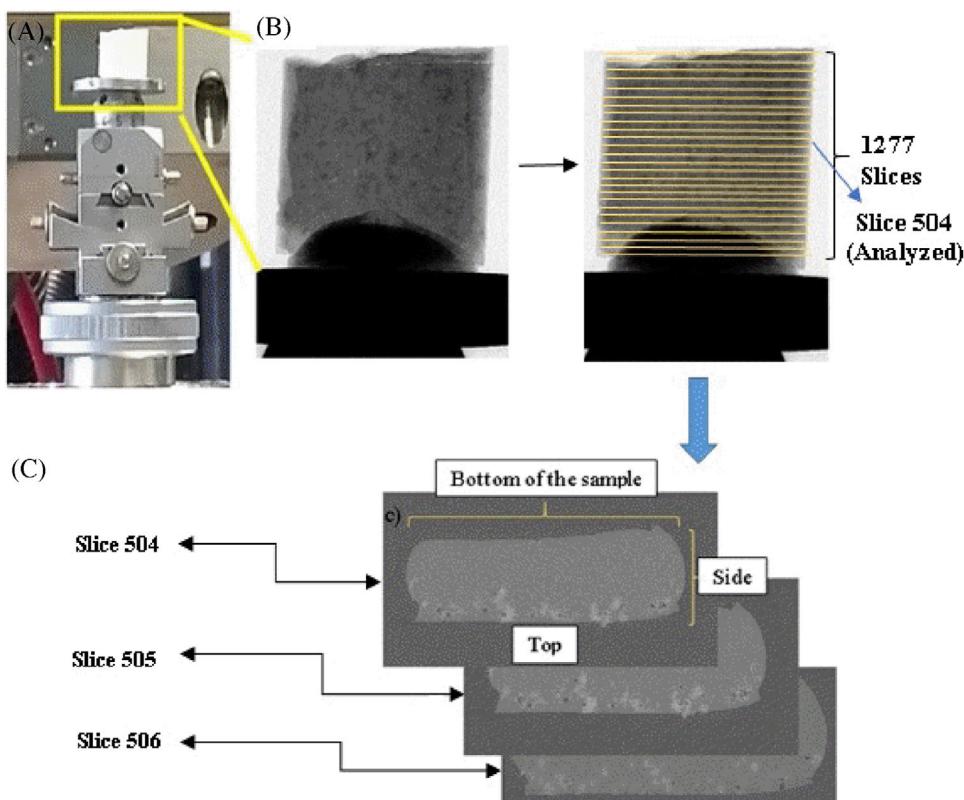**FIGURE 11**   Projection obtained during the rotation of the sample in 360°

FIGURE 12   A, Self-healing sample in the rotation stage; B, 2D X-ray images (projections) obtained during the rotation of the sample; C, image reconstruction in 2D cross sections (in z direction)

considerably less microcapsules in the 60-120 μm range. For filled microcapsules, the average particle size was 31 ± 17 μm (Figure 14A). The number of filled particles is higher than hollow microcapsules, that is, most of the microcapsules remain intact within the polymer matrix. However, there is a drop in the number of microcapsules with diameters over 60 μm, which is even more pronounced above 80 μm, where only a few microcapsules remain. The amount of deformed microcapsules and clusters, now choosing a value far from circularity, is shown in Figure 14B. Particle sizes between 100 and 150 μm can be attributed to filled microcapsules with irregular forms, while particles in the 150-500 μm range are related to clusters—most of them near the sample surface.
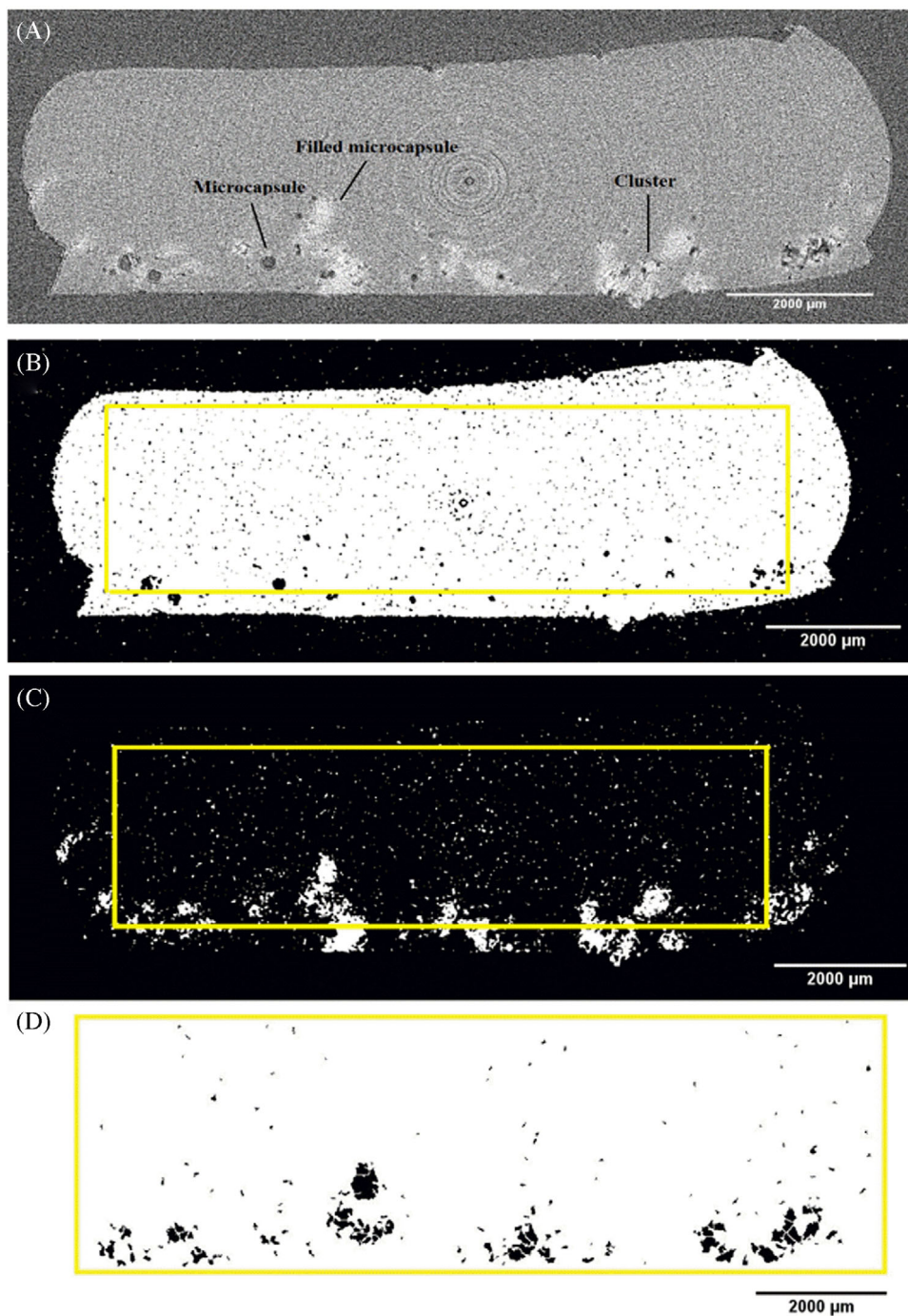
FIGURE 13 A, μCT slice of the specimen, where the microcapsules are concentrated on the polymer surface (the arrows highlight hollow and filled microcapsules and a cluster); B, the grayscale image of Figure 5A transformed into binary; C, filled microcapsules extracted by selecting a gray level value of 175 and a circularity values from 0.8 to 1.0; D, clusters extracted by selecting gray level values >175 and circularity values from 0.3 to 0.7

The results show interesting points: most of the microcapsules with diameters <60 μm are spherical, remain intact within the matrix, and practically do not form clusters. It is known that the thickness of the microcapsule shell decreases as the diameter of the microcapsule increases.[31] As microcapsules of smaller diameters have a higher surface-to-diameter ratio, urea-formaldehyde (UF) particles are deposited in larger quantities on the surface of the microcapsule, increasing its thickness. The increase in the microcapsules thickness is an advantage since the microcapsule does not rupture easily during the polymer processing.[38,39]
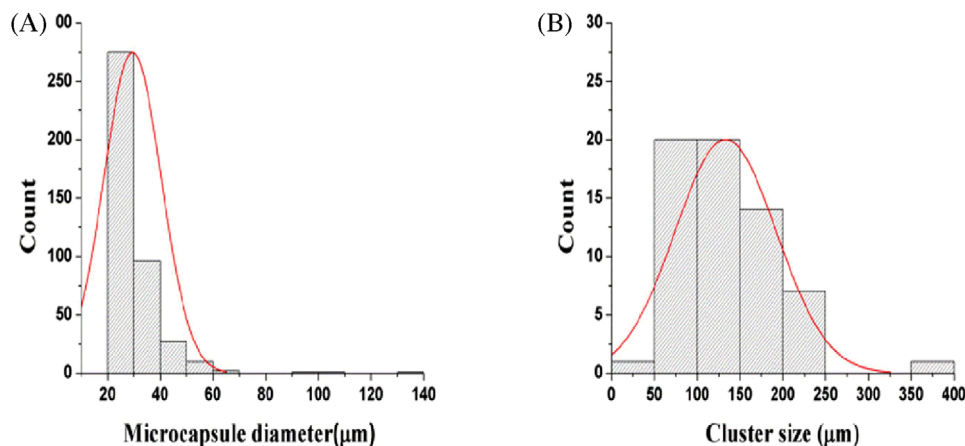
FIGURE 14 A, Microcapsule size distribution of embedded PUF microcapsules filled with PDMS-a, with circularity values ranging from 0.8 to 1.0; B, "particles" with circularity values between 0.3 and 0.7, considered as clusters
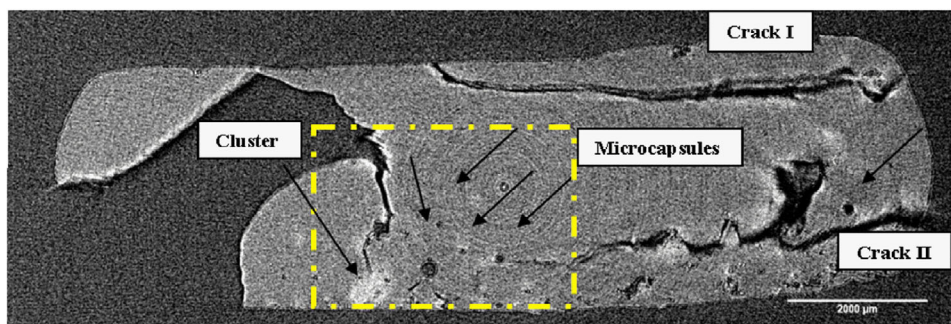
FIGURE 15 A horizontal cross-section of the epoxy matrix with microcapsules near the fracture surface. The fracture caused cracks (I and II) through the epoxy matrix. The black arrows indicate stress-ruptured microcapsules. The region highlighted by the yellow box is studied in more details in Figure 16

## 3.4 | Crack investigation and the self-healing mechanism

3.4.1 | μCT analysis

The purpose of a self-healing material is to close a crack autonomously. One of the possible approaches for polymer materials is the dispersion of microcapsules filled with healing agents into the polymer matrix, which shell should be easily ruptured by a propagating crack. It is also necessary for the released healing agent to react quickly to close the fracture on time, preventing the crack from growing until the failure of the material. To study this system, in Figure 15 is presented a slice of the self-healing specimen below the fracture surface. There are two main cracks in the polymer matrix. The crack *I* is located on the bottom of the sample, and the crack *II* is located near its surface. Microcracks are also present and highlighted by the yellow area. The healing process stopped the crack *II* from spreading, as pointed by the three black arrows.

The sequence of images in Figure 16 illustrates a more detailed study of the self-healing process occurring in the region highlighted in Figure 15. The crack-tip point and crack growth were monitored through a sequence of images at different slice positions. On the left side of Figure 16-T1, a crack reaches a cluster of microcapsules (A). At the center of the image, a filled microcapsule (B) and a ruptured microcapsule (C) appear in the polymer matrix. As different information takes place simultaneously, each event will be discussed apart in the next sections.

Event A

Figure 16-T1 shows, on the left side of the slice, a crack that reaches a cluster of microcapsules. In Figure 16-T4, the *arrow I* points to a white area where the healing agent was released from a ruptured microcapsule. *Arrow II* leads to the region where the crack is being healed by the healing agent released both from the cluster and from a nearby dispersed microcapsule. It is observed that the healing process was efficient in interrupting the crack growth and a considerable decrease in the crack extension, although the
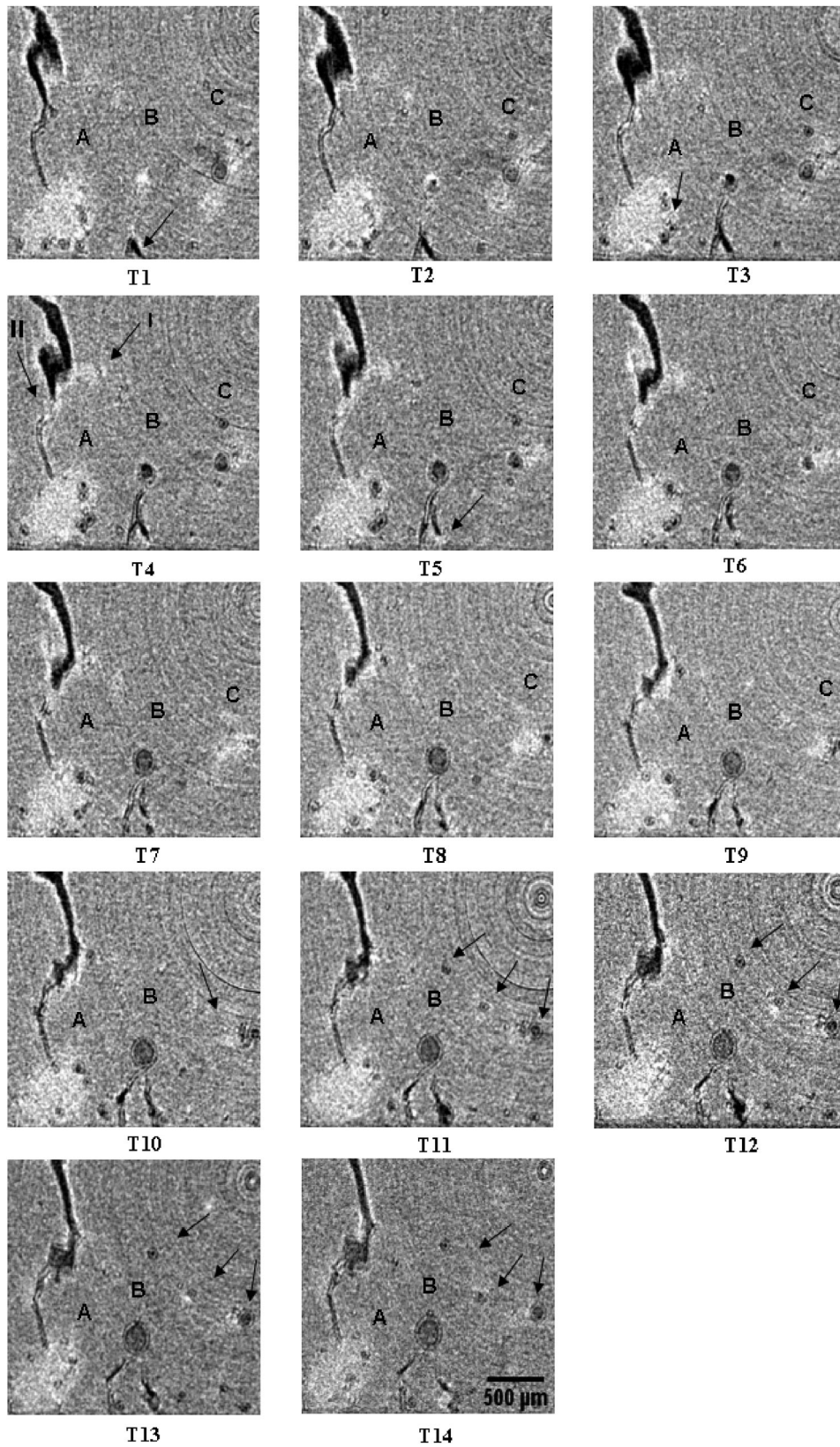
FIGURE 16   A sequence of slices from a μCT scan showing PDMS-a filled microcapsules dispersed within the epoxy matrix. Each slice shows a position within the sample, starting in the slice 0453-0440. Region A highlights a crack that reaches a cluster of microcapsules, while regions B, and C indicate filled microcapsules being ruptured within the matrix
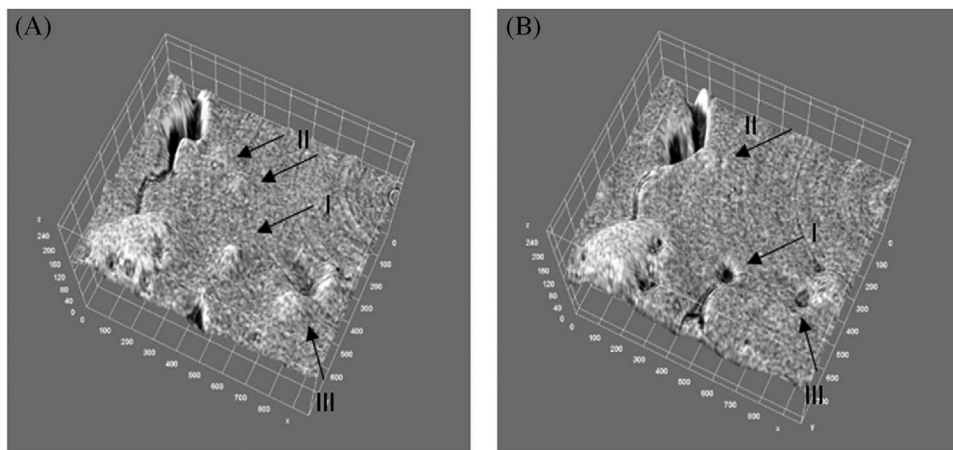
FIGURE 17 3D plotting of the slice surface from T1. The light gray spots, pointed by arrows I, II, and III are microcapsules. The two raised areas highlighted by arrow II are microcapsules not visible in a 2D image. These microcapsules are responsible for the release of the PDMS-a in the crack area in Figure 13-T4, arrow I; B, 3D plotting of the slice surface of T4, showing a cavities after the release of the healing agent (arrows II and III)

amount of healing agents released by microcapsules was not enough to fully close the crack.

Event B

The arrow points to a crack starting below the microcapsule (B) in Figure 16-T1 that is advancing in Figure 16-T2 until the microcapsule ruptures in Figure 16-T3. The liquid released spread over the crack area started the healing process (Figure 16-T5). The microcrack stops to grow, being almost completely healed (Figure 16-T12).
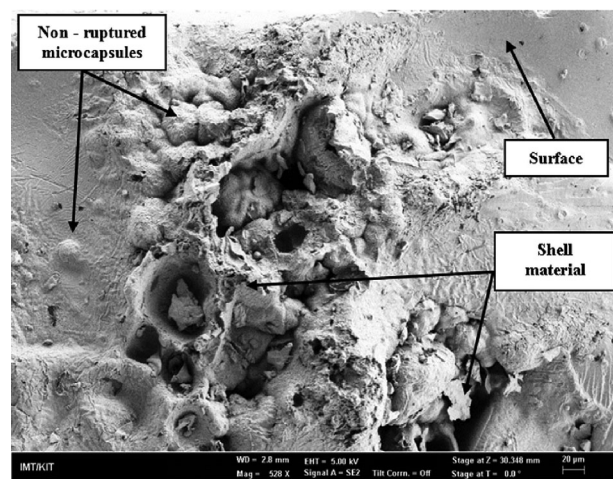
Event C

The healing agent released from ruptured microcapsule C can be identified by a light gray area around it (Figure 16-T1). The healing process continues until the microcapsule region is thoroughly closed in Figure 16-T7. Another smaller microcapsule (Figure 16-T8) is ruptured near the microcapsule C by the growth of microcrack *II* (Figure 15, II). Two other microcapsules on the way of the microcrack *II* are also broken (Figure 16-T11).

A 3D plot of the slice surface of Figure 16-T1 confirms that the light-gray level points are microcapsules. Figure 17A shows the microcapsules as elevated white points, specified by *arrows I, II, and III*. It can be noticed that, after reaching the cracks, the microcapsules break, releasing the healing agent and forming cavities at those points (Figure 17B).

3.4.2 | Scanning electron microscopy

SEM images of fracture surface, Figures 18 and 19, give information about crack tip position, microcapsules size, microcapsules adhesion to the polymer matrix, and the release of the healing agent. Furthermore, it is possible, even in a small piece of the sample, to correlate this infor-


FIGURE 18 SEM image of the fracture surface showing a cluster formed by shell material from ruptured microcapsules. This SEM image in full scale and high resolution is available in Supporting Information, Section S4. Events B and C

mation with μCT analyses, avoiding a wrong interpretation of the data. The investigation will be divided into events A, B, and C, as used in Figure 16, to consider the same regions of interest.

Event A

A SEM image of the fracture surface of the same self-healing specimen analyzed by μCT is presented in Figure 18, showing that, near to the surface of the sample, the cluster is made by microcapsules that remain intact and the shell material of ruptured microcapsules, confirming the tomography analysis. The shell material goes to the surface because the density of PUF is lower than that of the polymer matrix.[45] Then, it agglomerates and can cause air trapping during the cure of the matrix. Clusters

FIGURE 19 SEM image of fracture surface of a self-healing specimen showing: A, broken microcapsules and healed regions around the crack; B, an unbound microcapsule and a healed region, and (C) a ruptured microcapsule and partial healing. The direction of the crack growth is from left to right
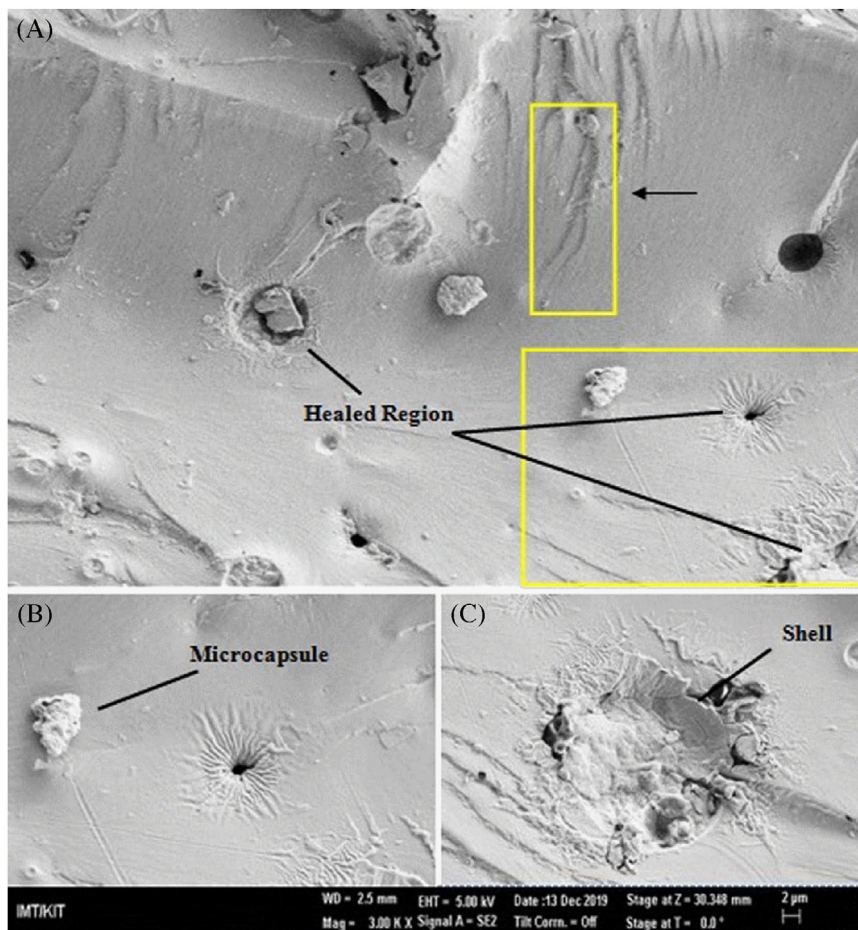
can prevent the advance of the crack; however, they can also act as stress points into the polymer matrix, decreasing its mechanical properties.[3] For better visualization of the microcapsules by μCT, in this work, a much higher amount of microcapsules were used (28 wt%), compared to our previous work (2.5 wt and 5.0 wt%),[17] leading to the observation of large clusters.

SEM images shows that the crack in Figure 16-T3 has the same pattern observed nearby the microcapsules (Figure 19A). It was observed that most of the microcapsules broke off during the fracture, releasing the healing agent. In some cases, the healing agent was capable of closing almost all the ruptured region, as highlighted in Figure 19A ("Healed Region"). Figure 19B presents an "unbound" microcapsule with a similar shape to that observed in Figure 9B. Figure 19C shows a ruptured microcapsule, allowing the visualization of its shell, and showing an adequate adhesion of the microcapsule with the polymer matrix. Around the microcapsules, there is a crimped region, which can be attributed to the partial healing process.[28,46] Observing the entire fracture region, the smooth appearance of the surface can be due to the induced toughening [47–50] that occurs using PDMS-a as healing agent (Figure 19). This information was confirmed through fracture

toughness tests in our previous work,[17] where the complete regenerating of fracture toughness was achieved.

4 | CONCLUSION

The self-healing triggering mechanism of an epoxy material, prepared using PUF microcapsules filled with an aminated polysiloxane (PDMS-a) as a healing agent, has been revealed by μCT and SEM. μCT in situ characterization allowed monitoring the crack growth until the rupture of the microcapsules and the crack closure. PDMS-a was effective in self-regenerating microcracks even at room temperature, confirming the fracture toughness results of our previous work. The results show that most of microcapsules with diameters larger than 60 μm (and shell thickness around 0.4 μm) are ruptured during dispersion into the epoxy matrix. In contrast, microcapsules with diameters smaller than 60 μm remain intact during the dispersion and curing of the epoxy resin. μCT and SEM analyses allowed relating the size of the microcapsules with superficial agglomerates. μCT and SEM images confirmed that the self-healing process occurs by a specific mechanism, including crack bowing and deflections when

approaching a microcapsule, indicating that the microcapsules are strongly adhered to the polymer matrix. This crack deflection mechanism explains the excellent results of fracture toughness obtained in previous work by the group for the same system. The results show that the use of μCT investigations, along with microscopy, enables the optimization of processing parameters of self-healing polymers, and the improvement of the performance of such materials.

CONFLICT OF INTEREST
The authors declare no conflict of interest.

DATA AVAILABILITY STATEMENT
The data that support the findings of this study are available from the corresponding author upon reasonable request.

REFERENCES

1. S. R. White, N. R. Sottos, P. H. Geubelle, J. S. Moore, M. R. Kessler, S. R. Sriram, E. N. Brown, S. Viswanathan, *Nature.* **2001**, *409*, 794.
2. E. N. Brown, N. R. Sottos, S. R. White, J. Moore, *Exp. Mech.* **2002**, *42*, 372.
3. E. N. Brown, S. R. White, N. R. Sottos, *J. Mater. Sci.* **2006**, *41*, 6266.
4. C. Wang, H. Wu, Z. Chen, M. T. McDowell, C. Yi, Z. Bao, *Nat. Chem.* **2013**, *5*, 1042.
5. L. Lv, E. Schlangen, Z. Yang, F. Xing, *Materials.* **2016**, *9*, 1025.
6. R. Wool, *Soft Matter.* **2008**, *4*, 400.
7. N. J. Kanu, E. Gupta, U. K. Vates, G. K. Singh, *Compos. Part A- Appl. S.* **2019**, *121*, 474.
8. Y. Deng, X. Liang, X. Pei, K. Zhai, C. Wang, B. Zhang, Y. Bai, Y. Zhang, P. Wang, Y. Tan, K. Xu, *Polym. Test.* **2019**, *76*, 43.
9. Y. Yang, G. Lei, J. Xie, Y. Zhou, J. Hu, Q. Li, J. He, *Nanoscale.* **2020**, *12*, 3605.
10. Y. Li, Z. Yang, J. Zhang, L. Ding, L. Pan, C. Huang, X. Zheng, C. Zeng, C. Lin, *Polym. Test.* **2019**, *76*, 82.
11. A. Mirmohseni, M. Akbari, R. Najjar, M. Hosseini, *J. Appl. Polym. Sci,* **2019**, *136*, 47082.
12. F. Zhang, L. Zhang, M. Yaseen, K. Huang, *J. Appl. Polym. Sci.* **2021**, *138*, 50260.
13. M. Korsali, D. G. Bekas, K. Tsirka, D. Baltzis, D. T. Vaimakis-Tsogkas, S. Orfanidis, G. Papavassiliou, *Compos. Part B Eng.* **2019**, *171*, 78.
14. J. Rule, N. Sottos, N. White, *Polymer.* **2007**, *48*, 3520.
15. S. Mostovoy, P. Crosley, E. Ripling, *J. Mater.* **1967**, *2*, 661.
16. Y. R. Lee, S. C. Kim, H. Lee, H. M. Jeong, A. V. Raghu, K. R. Reddy, B. K. Kim, *Macromol. Res.* **2011**, *19*, 66.
17. W. R. Weihermann, M. M. Meier, S. H. Pezzin, *J. Appl. Polym. Sci.* **2019**, *136*, 47627
18. C. Mangun, A. Mader, N. Sottos, S. White, *Polymer.* **2010**, *51*, 4063
19. M. R. Kessler, S. R. White, *Compos A- Appl. Sci. Manuf.* **2001**, *32*, 683.
20. M. R. Kessler, N. R. Sottos & S. R. White *Compos A- Appl. Sci. Manuf.* **2003**, *34*, 743.
21. W. Sima, Q. Shao, P. Sun, C. Liang, M. Yang, Z. Yin, Q. Deng, *Chem. Eng. J.* **2021**, *405*, 126908.
22. M. Clausi, I. S. Bayer, *Nano Select.* **2021**, *2*, 433.
23. A. H. Navarchian, N. Najafipoor, F. Ahangaran, *Prog. Org. Coat.* **2019**, *132*, 288.
24. M. R. Kessler, *Proc. IMechE Part G: J. Aerosp. Eng.* **2007**, *22*, 479.
25. J. V. Stappen, T. Bultreys, F. A. Gilabert, X. K. Hillewaere, D. G. Gómez, K. V. Tittelboomd, J. Dhaene, N. D. Belie, W. V. Paepegem, F. E. D. Prez, V. Cnudde, *Mater. Charact.* **2016**, *119*, 99.
26. C. S. Mayo, A. W. Stevenson, S. W. Wilkins, *Materials.* **2012**, *5*, 937.
27. C. S. Mayo, A. Stevenson, S. Wilkins, D. Gao, S. Mookhoek, S. Meure, T. Hughes, J. Mardel, *Mater. Sci. Forum.* **2010**, *654*, 2322.
28. S. D. Mookhoek, S. C. Mayo, A. E. Hughes, S. A. Furman, H. R. Fischer, S. van der Zwaag, *Adv. Eng. Mater.* **2010**, *12*, 228.
29. M. Peñas-Caballero, M. H. Santana, R. Verdejo, M. A. Lopez-Manchado, *React. Funct. Polym.* **2021**, *161*, 104847.
30. S. McDonald, S. Coban, N. Sottos, P. Withers, *Sci. Rep.* **2019**, *9*, 1.
31. E. N. Brown, M. R. Kessler, N. R. Sottos, S. R. White, *J. Microencapsul.* **2003**, *20*, 719.
32. B. Blaiszik, N. Sottos, W. S. R., *Compos. Sci. Technol.* **2008**, *68*, 978.
33. H. Jin, C. L. Mangun, D. S. Stradley, J. S. Moore, N. R. Sottos, S. R. White, *Polymer.* **2012**, *53*, 581.
34. M. Berger, J. Hubbell, S. Seltzer, J. Chang, J. Coursey, R. Sukumar, D. Zucker, K. Olsen, XCOM: Photon Cross Sections Database, National Institute of Standards and Technology, **2010**, [Online]. Available: http://physics.nist.gov/xcom, Accessed: February, 2020.
35. G. Fang, Y. Liu, S. Qin, W. Ding, J. Zhang, S. Hong, F. Xing, B. Dong, *Constr. Build. Mater.* **2018**, *179*, 336.
36. B. Blaiszik, S. Kramer, S. Olugebefola, J. Moore, N. Sottos, S. White, *Annu. Rev. Mater. Res.* **2010**, *40*, 179.
37. W. Zhang, L. Liao, Y. Zhao, in *Handbook of Smart Coatings for Materials Protection*, (Eds: A. S. H. Makhlouf),Woodhead, **2014**, *12*, 287.
38. M. D. L. P. Miguel, R. Ollier, V. Alvarez, C. Vallo, *Prog. Org. Coat.* **2016**, *97*, 194.
39. C. Fan, X. Zhou, *Colloid Surface A.* **2010**, *363*, 49.
40. R. P. Ollier, E. M. PenoffV, V. A. Alvarez, *Colloid Surface A.* **2016**, *51*, 27.
41. P. A. Bolimowski, I. P. Bond, D. F. Wass, *Phil. Trans. R. Soc. A.* **2015**, *374*, 20150083.
42. R. A. Chowdhury, M. V. Hosur, M. Nuruddin, A. T. Narteh, A. Kumar, V. Boddu, S. Jeelani, *J. Mater. Res. Technol.* **2015**, *4*, 33.

43. S. Fidan, in *Micro-computed Tomography (micro-CT) in Medicine and Engineering*, (Ed: K. Orhan), Springer, **2020**, *16*, 267.

44. G. Kiziltaş, M. Papila, B. Yilmaz, K. Bilge, in *Micro-computed Tomography (micro-CT) in Medicine and Engineering*, (Ed: K. Orhan), Springer, **2020**, *16*, 225.

45. M. Keller, N. Sottos, *Exp. Mech.* **2006**, *46*, 725.

46. S. D. Mookhoek, in *Novel routes to liquid-based self-healing polymer systems*, Eindhoven, Technische Universiteit Delft, **2010**, *4*, 47.

47. M. Tripathi, D. K. Rahamtullah, C. Rajagopal, P. K. Roy, *J. Mater. Sci.* **2014**, 131.

48. T. Yin, M. Z. Rong, M. Q. Zhang, G. C. Yang, *Compos. Sci. Technol.* **2007**, *67*, 201.

49. S. Cho, H. Andersson, S. White, N. Sottos, P. Braun, *Adv. Mater.* **2006**, *18*, 997.

50. E. Brown, S. White, N. Sottos, *J Mater Sci.* **2004**, *39*, 1703.

SUPPORTING INFORMATION

Additional supporting information may be found online in the Supporting Information section at the end of the article.